COBEM 2023 27TH INTERNATIONAL CONGRESS OF MECHANICAL ENGENEERING

ABCM Brazilian Society of Mechanical Sciences and Engineering
27th ABCM International Congress of Mechanical Engineering
December 04-08, 2023, Florianópolis-SC, Brazil

COB-2023-1071
RECURSIVE HEAT FLUX ESTIMATION IN NONLINEAR HEAT CONDUCTION USING KALMAN FILTER AND KIRCHHOFF TRANSFORM

Arthur S. M. Anastácio
César C. Pacheco
Department of Mechanical Engineering, Federal Fluminense University (PGMEC/UFF)
cesarp@id.uff.br

Abstract. *This paper deals with the problem of estimating high-magnitude heat fluxes applied at the surface of a flat plate. The inverse problem is solved by assuming that transient temperature measurements are available at the opposite side of the plate. Previous works have shown that solution methodologies based on Kalman filtering and reduced-order modelling are capable of yielding estimates in good agreement with reference values. However, since this reduced-order model assumes constant thermal properties, when high temperatures are achieved, the onset of physical nonlinearities lead to inaccurate results. To address this issue, the Kalman Filter is rewritten, now considering the heat conduction model in terms of the Kirchhoff transform, which addresses partially these nonlinearities, alleviating this modelling errors up to a certain degree. The inverse problem was proposed in this approach as a state variable estimation problem, typical of dynamical systems such as the mathematical model of the direct problem. The solution of the direct problem was written in the form of an evolution-observation model (EOM), in its linear form, according to the equations resulting from the Finite Volume (FVM) analysis. The proposed approach requires only the assumption of constant thermal diffusivity, allowing for some variation in the thermal conductivity and thermal capacity.*

Keywords: *inverse problems, state estimation, heat conduction*

1. INTRODUCTION

In the realm of engineering problems, one often encounters a problem of evaluating certain quantities that lie beyond the reach of direct measurement. The possible kinds of impediments are manifold, including hazardous environments for probe placement or geometrical inaccessibility. To address this issue, one may resort to indirect measurements, by means of solving an inverse problem. Such an approach bestows upon us the ability to estimate unknown quantities in mathematical models, encompassing physical properties or boundary/initial conditions, by means of experimentally measuring its output. Verily, inverse problems are not devoid of hardships of their own, for calculating its solution is both challenging and burdensome. The former refers to the fact that inverse problems are ill-posed, contrary to Hadamard (1902) definition of a well-posed problem, whose solution i) exists; ii) is unique; iii) is stable regarding input data. This state of ill-posedness implies falling short of meeting at least one of these conditions, specially the latter, which emerges as a matter of utmost concern, as the input data in this case comprises experimental observations, intrinsically affected with noise (Ozisik and Orlande, 2021). Henceforth, it becomes imperative to employ special techniques.

A practical example is the cooling of electronics, which is a problem of steadily increasing interest in engineering. The increase in processing power of microchips yields an ever increasing in power dissipation, so that the necessity emerges for more efficient methodologies for thermal management. Failing to do so can only lead to the microchip attaining temperatures beyond its material limitations, thus destroying the component. Proposals on improving thermal management in electronic boards can be found, for example, in the work of Abdoli et al. (2015), with different geometries being tested for micro pin-fins. This methodology was later the subject of optimization analyses from Reddy and Dulikravich (2017), in which optimal characteristic lengths were selected for the proposed geometries.

Verily, an important step in designing efficient cooling systems is accurately quantifying the heat loads to which the electronic board is subjected. In fact, this can be achieved by means of solving an inverse heat transfer problem, by taking temperature measurements in a given region of the board. Nevertheless, this type of analysis suffers from typically high computational loads, which may delay the quantification of the sought information. A proposed solution was given by Pacheco et al. (2016) by employing the Steady-State Kalman Filter (SSKF) (Simon, 2006) to the reduced model presented by Orlande et al. (2013), yielding a framework where the boundary heat flux is estimated at real-time. On the other hand, when large temperature ranges are present, their effect on the thermal properties are such that the reduced model fails to provide accurate estimates. This difficulty was addressed by Pacheco et al. (2015), with inclusion of the Approximation Error Model (AEM) (Huttunen and Kaipio, 2007) in the classical Kalman Filter. Yet, this technique requires sampling the reduced model and a support (herein called complete) model for calculation of the approximation errors, providing a

significant increase in the computational effort. Furthermore, the AEM could only be employed in the SSKF if the covariance matrix of the approximation errors is constant in time – which is often not the case.

It is undeniable that a major challenge in this problem is the temperature effect on the thermal properties – namely the thermal conductivity and capacity. In such scenario, this paper proposes to address the aforementioned difficulties by including the Kirchhoff Transform (KT) (Kakac et al., 2018). This technique slightly modifies the heat conduction equation, linearizing the diffusive operator. It is true that the thermal diffusivity remains as a function of the temperature in the model, but even if one linearizes this model by assuming it to be constant, a small room is present for changes in the thermal conductivity and capacity. As it will be shown in this paper, this increase in robustness allows for improvements on the quality of the estimates when high-magnitudes heat fluxes are present.

2. FORWARD PROBLEM

The physical model considered herein draws its foundation from the seminal works of Orlande (2013) and Pacheco (2015, 2016), the temperature $T(\mathbf{r},t)$ in a flat plate, shown in Figure 1, is to be assessed. This temperature is assumed to be a function of the time t and the position vector $\mathbf{r} = \{[x \quad y \quad z]^T \colon 0 < x < a,\ 0 < y < b,\ 0 < z < c\}$, the latter defining the domain Ω. Furthermore, the top boundary $\partial\Omega_1 = \{\mathbf{r} \in \Omega \mid z = c\}$ is heated by a focused high-magnitude heat flux $q(\mathbf{r},t)$, while the remaining boundaries, herein named as $\partial\Omega_2$ are kept insulated thermally. At last, the thermal properties of the plate are considered as functions of temperature and its initial temperature distributions is assumed uniform and equal to T_0.

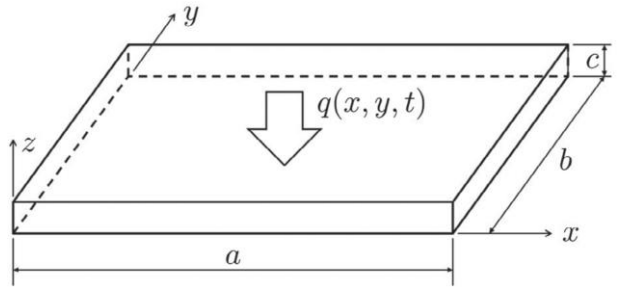

Figure 1. Physical model considered in this work (Pacheco et al., 2016).

This physical model is mathematically written in Eqs. (1)-(4), the former being the governing equation, the latter being the initial condition, and the remaining ones being the boundary conditions if imposed heat flux and thermal insulation, respectively.

$$C(T)\frac{\partial T}{\partial t} = \nabla \cdot [k(T)\nabla T], \qquad \mathbf{r} \in \Omega, t > 0; \tag{1}$$

$$k(T)\frac{\partial T}{\partial \mathbf{n}} = q(\mathbf{r},t), \qquad \mathbf{r} \in \partial\Omega_1, t > 0; \tag{2}$$

$$\frac{\partial T}{\partial \mathbf{n}} = 0, \qquad \mathbf{r} \in \partial\Omega_2, t > 0; \tag{3}$$

$$T(\mathbf{r},t) = T_0, \qquad \mathbf{r} \in \Omega, t = 0. \tag{4}$$

The temperature-dependent thermal properties of the plate are given by Eqs. (5) and (6) below.

$$k(T) = 12.45 + 0.014T + 2.517 \times 10^{-6}T^2 \ [\mathrm{Wm^{-1}K^{-1}}]; \tag{5}$$

$$C(T) = 1324.75T + 3557900 \ [\mathrm{Jm^{-3}K^{-1}}]. \tag{6}$$

After presenting this mathematical model, it becomes apparent that solving the proposed inverse analysis consists of assessing the unknown $q(\mathbf{r},t)$ applied at the top of the plate by using experimentally measured values of temperature at the plate bottom. Nevertheless, despite being comprehensive and robust, this model imposes a challenge within the inverse analysis, as its complexity yields an unfeasible computational effort. To address it, we resort to a reduced order model, obtained via averaging the temperature in the z direction, in addition to an improved lumped analysis (Cotta and Mikhailov, 1997) to model the respective temperature gradients more appropriately. In this model, the average temperature $\overline{T}(\overline{\mathbf{r}},t)$ is a function of time t and of the position vector $\overline{\mathbf{r}} = \{[x \quad y]^T \colon 0 < x < a,\ 0 < y < b\}$, which defines the domain $\overline{\Omega}$. Also, this model assumes constant thermal properties, its values obtained from evaluating Eqs. (5) and (6) at a reference temperature T^* herein considered to be 600 K – that is, $C^* = C(T^*)$ and $k^* = k(T^*)$. Therefore, the reduced order model is given by Eqs. (7)-(10), where the heat flux appears as a source term.

$$C^* \frac{\partial \overline{T}}{\partial t} = k^* \frac{\partial^2 \overline{T}}{\partial x^2} + k^* \frac{\partial^2 \overline{T}}{\partial y^2} + \frac{q(x,y,t)}{c}, \quad \overline{\mathbf{r}} \in \overline{\Omega}, t > 0; \tag{7}$$

$$\frac{\partial \overline{T}}{\partial x} = 0, \qquad x = 0 \text{ and } x = a, t > 0; \tag{8}$$

$$\frac{\partial \overline{T}}{\partial y} = 0, \qquad y = 0 \text{ and } y = b, t > 0; \tag{9}$$

$$\overline{T} = T_0, \qquad \overline{\mathbf{r}} \in \overline{\Omega}, t = 0. \tag{10}$$

However, since the experimental measurements are assumed available at the top surface of the place (that is, the $z = c$ plane), it becomes a necessity to appropriately describe it in terms of the average temperature $\overline{T}$. Such relation is achieved through the improved lumped formulation, yielding Eq. (11) (Orlande et al., 2013; Pacheco et al., 2015). This linear, two-dimensional model is significantly less intensive computationally, thus rendering possible an inverse analysis.

$$T(x,y,z=0,t) = \overline{T}(x,y,t) - \frac{c}{6k^*} q(x,y,t). \tag{11}$$

As mentioned above, this setup has been the subject of past publications. In these, good agreement was achieved between reference and estimated quantities. Yet should one increase the time frame of the analysis, the assumptions in the reduced models lose adherence, leading to the onset of significant errors. To overcome this challenge, we resort to the Kirchhoff Transform (KT) (Kakac et al., 2018), which can be described via Eqs. (12) or (13). This technique relies in defining a reference temperature, herein considered to be the same T^* defined above.

$$k(T)dT = k^* d\theta; \tag{12}$$

$$\theta(\mathbf{r},t) = \theta_{\text{ref}} + \frac{1}{k^*} \int_{T^*}^{T(\mathbf{r},t)} k(T)dT\,. \tag{13}$$

Should one apply KT to the complete model (cf. Eqs. (1)-(4)) and proceed with the model reduction proposed by Orlande et al. (2013), a similar reduced model arises, as shown below in Eqs. (14)-(17), where it is no longer required to assume both the thermal conductivity and heat capacity to be constants, but only the thermal diffusivity, here deemed as $\alpha^* = \alpha(T^*)$, with $\alpha(T) = k(T)/C(T)$. It follows then that this approach can permit some variation in k and C, with the condition that α does not change significantly. We understand this to be a significant step in improving the robustness of the reduced model, leading to better results in the inverse analysis.

$$\frac{1}{\alpha^*} \frac{\partial \overline{\theta}}{\partial t} = \frac{\partial \overline{\theta}}{\partial x^2} + \frac{\partial \overline{\theta}}{\partial y^2} + \frac{q(x,y,t)}{ck^*}, \qquad \mathbf{r} \in \overline{\Omega}, t > 0; \tag{14}$$

$$\frac{\partial \overline{\theta}}{\partial x} = 0, \qquad x = 0 \text{ and } x = a, t > 0; \tag{15}$$

$$\frac{\partial \overline{\theta}}{\partial y} = 0, \qquad y = 0 \text{ and } y = b, t > 0; \tag{16}$$

$$\overline{\theta} = \theta_0, \qquad \overline{\mathbf{r}} \in \overline{\Omega}, t = 0; \tag{17}$$

$$\theta(x,y,z=0,t) = \overline{\theta}(x,y,t) - \frac{c}{6k^*} q(x,y,t). \tag{18}$$

At last, we address the numerical solution of the complete and reduced models. The Finite Volume Method (FVM) (Versteeg and Malalasekera, 2007) was employed to discretize the spatial derivatives in a numerical grid with $n_x n_y$ control volumes. The resulting system of coupled ordinary differential equations was integrated using explicit Euler integration with time step Δt. The said discretization process is herein omitted for the sake of brevity. Yet, this discretized model will be again referred to in the following section.

3. INVERSE PROBLEM

An indispensable element of the envisioned analysis resides in being capable of estimating the heat flux distribution *online*, that is, recursively, as new information arrives. Therefore, this work traverses the path paved by prior publications, recasting this inverse problem as a state estimation problem (Orlande et al., 2012). In this sense, we define the state vector $\mathbf{x}_k$ to contain both the average temperature values throughout the numerical grid, as well as the respective local heat flux values, resulting in a state vector with $2n_x n_y$ state variables. As for the observation vector $\mathbf{y}_k$, it has a size of $n_x n_y$, referring to the temperature values observed at the $z = 0$, calculated by means of Eq. (18).

In state estimation problems, it is paramount to define the evolution-observation model (EOM), which describes how the state vector evolves over time and how the observed quantities are obtained from it. We assume herein this model to be linear and according to Eqs. (19) and (20), where $\mathbf{w}_{k+1}$ and $\mathbf{v}_k$ are random Gaussian vectors, with zero mean and covariance matrices $\mathbf{Q}_k$ and $\mathbf{R}_k$, respectively, the former codifying the uncertainties in the model and the latter modelling the experimental noise. The state evolution matrix $\mathbf{F}_k$ is obtained precisely from the Euler integration of the system of ODEs resulting from the FVM discretization, while the observation matrix $\mathbf{H}_k$ follows from appropriately mapping $\mathbf{x}_k$ to $\mathbf{y}_k$ by means of Eq. (18).

$$\mathbf{x}_{k+1} = \mathbf{F}_k\mathbf{x}_k + \mathbf{w}_{k+1}; \tag{19}$$
$$\mathbf{y}_k = \mathbf{H}_k\mathbf{x}_k + \mathbf{v}_k. \tag{20}$$

The solution of the linear state estimation problem given above is obtained analytically and it is known as the Kalman Filter (Kalman, 1960; Chen, 2003; Simon, 2006), whose equations are shown below. Therein, we have the *prior* and *posterior* estimates of the state vector $\hat{\mathbf{x}}_k^-$ and $\hat{\mathbf{x}}_k^+$, respectively; the *prior* and *posterior* estimation error covariance matrices $\mathbf{P}_k^-$ and $\mathbf{P}_k^+$, respectively; and the Kalman gain matrix $\mathbf{K}_k$. The implementation of such equations is straightforward, most of the time involving matrix-vector and matrix-matrix multiplications. Yet, as shown in Eq. (23), a matrix inversion must take place at each recursion (that is, time step), which might yield computationally intensive steps throughout the solution, which is an undesirable feature when real-time estimation is sought.

$$\hat{\mathbf{x}}_k^- = \mathbf{F}_k\hat{\mathbf{x}}_{k-1}^+; \tag{21}$$
$$\mathbf{P}_k^- = \mathbf{F}_k\mathbf{P}_{k-1}^+\mathbf{F}_k^T + \mathbf{Q}_k; \tag{22}$$
$$\mathbf{K}_k = \mathbf{P}_k^-\mathbf{H}_k^T[\mathbf{H}_k\mathbf{P}_k^-\mathbf{H}_k^T + \mathbf{R}_k]^{-1}; \tag{23}$$
$$\hat{\mathbf{x}}_k^+ = \hat{\mathbf{x}}_k^- + \mathbf{K}_k[\mathbf{y}_k - \mathbf{H}_k\hat{\mathbf{x}}_k^-]; \tag{24}$$
$$\mathbf{P}_k^+ = (\mathbf{I} - \mathbf{K}_k\mathbf{H}_k)\mathbf{P}_k^-. \tag{25}$$

It so happens, that this EOM is not only linear, but time invariant as well. This implies that the structure of its matrices does not change over time – that is, $\mathbf{F}_k \simeq \mathbf{F}$, $\mathbf{H}_k \simeq \mathbf{H}$, $\mathbf{Q}_k \simeq \mathbf{Q}$, $\mathbf{R}_k \simeq \mathbf{R}$. Such scenario means that the error covariance and Kalman gain matrices behave asymptotically, so that over time $\mathbf{K}_k \simeq \mathbf{K}_\infty$ and $\mathbf{P}_k^- \simeq \mathbf{P}_k^+ \simeq \mathbf{P}_\infty$ (Simon, 2006). Therefore, it is expected that, should one approximate the error covariance and Kalman gain matrices by their asymptotic values, the computational burden might decrease severely. Verily, the consequence of such an approach is to reduce the classical Kalman filter to Eqs. (26)-(28), which are known as the Steady-State Kalman Filter (SSKF) (Simon, 2006). This technique presents a significant advantage when compared to the classical Kalman filter, as only Eq. (28) depends on either the measurements or the state estimates. The two remaining equations depend only on the matrices of the EOM, meaning that $\mathbf{P}_\infty$ and $\mathbf{K}_\infty$ can be determined before the state estimation itself takes place. It bears note as well that these two equations carry most of the computational effort involved. In result, the SSKF achieves a scenario where the most intensive calculations are made in a preprocessing step before any measurements are processed. At the time of indeed solving the state estimation problem, one is faced with just Eq. (28), which comprises just simple linear algebra operations.

$$\mathbf{P}_\infty = \mathbf{F}\mathbf{P}_\infty\mathbf{F}^T - \mathbf{F}\mathbf{P}_\infty\mathbf{H}^T(\mathbf{H}\mathbf{P}_\infty\mathbf{H}^T + \mathbf{R})^{-1}\mathbf{H}\mathbf{P}_\infty\mathbf{F}^T + \mathbf{Q}; \tag{26}$$
$$\mathbf{K}_\infty = \mathbf{P}_\infty\mathbf{H}^T(\mathbf{H}\mathbf{P}_\infty\mathbf{H}^T + \mathbf{R})^{-\mathbf{1}}; \tag{27}$$
$$\hat{\mathbf{x}}_k^+ = (\mathbf{I} - \mathbf{K}_\infty\mathbf{H})\mathbf{F}\hat{\mathbf{x}}_{k-1}^+ + \mathbf{K}_\infty\mathbf{y}_k. \tag{28}$$

The covariance matrices related to the Gaussian noise vectors in Eqs. (19) and (20) are herein assumed to be diagonal and given according to Eqs. (29) and (30), respectively. In these, σ_y stands for the standard deviation of the experimentally measured temperatures, while σ_T represents the standard deviation of the uncertainties in the reduced model. On the other hand, we model the heat flux in the EOM by means of a random-walk model, so that σ_q is its standard deviation. Therefore, selecting σ_q implies a tradeoff between the algorithm responsiveness to sudden changes in the heat flux state variables and the uncertainties of their estimates. Their values will be the subject of discussion in the results section next.

$$\mathbf{Q} = \begin{bmatrix} \sigma_T^2\mathbf{I} & \mathbf{0} \\ \mathbf{0} & \sigma_q^2\mathbf{I} \end{bmatrix}; \tag{29}$$
$$\mathbf{R} = \sigma_y^2\mathbf{I}. \tag{30}$$

4. RESULTS

4.1 Preliminaries

4.1.1 Simulating synthetic measurements

First and foremost, it bears stressing that we sought in this work to test the proposed methodology robustness in a scenario as close as possible to a real situation. To this end, despite all measurements herein considered being synthetic, they are free of inverse crime, being obtained from the solution of the complete, nonlinear and three-dimensional model using a converged grid. For the sake of clarity, we shall henceforth refer to this model as the forward problem. In the state estimation problem, we considered the reduced model with KT discussed above, in a grid with $n_x = n_y = 24$, thus resulting in a grid with 576 control volumes and 1152 state variables.

Noise addition to the synthetic measurements was performed according with Eqs. (31), where $\mathbf{y}_k^e$ is the solution of the forward problem using the reference heat flux (which we will thereafter seek reconstructing) and $\boldsymbol{\omega}$ is a Gaussian random vector (cf. Eq. (32)), which was samples using LAPACK subroutine DLARNV.

$$\mathbf{y}_k = \mathbf{y}_k^e + \boldsymbol{\omega}; \tag{31}$$

$$\boldsymbol{\omega} \sim N(\mathbf{0}, \mathbf{R}). \tag{32}$$

4.1.2 Description of the numerical experiments

To evaluate the robustness of the devised methodology, we designed numerical experiments similar to those from past publications (Orlande et al., 2013; Pacheco et al., 2015, 2016), in order to properly test the effectiveness of including KT. In these, a $120 \times 120 \times 3$ mm plate is considered, with a high-magnitude, focused heat flux applied, its distribution given by Eq.(33) and depicted in Figure 2. That is, $x_0 = y_0 = 40$ mm and $x_1 = y_1 = 50$ mm.

$$\frac{q(x,y,t)}{q_0} = \begin{cases} 1, & x_0 < x < x_1 \text{ and } y_0 < y < y_1 \\ 0, & \text{otherwise} \end{cases}. \tag{33}$$

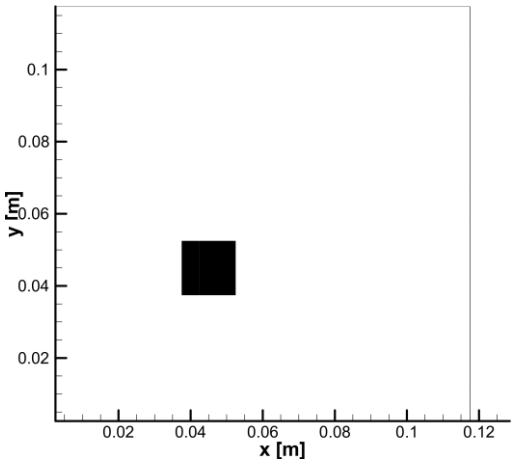

Figure 2. Reference heat flux distribution considered in the numerical experiments.

Furthermore, the numerical experiments differ between themselves in the value selected for q_0, as shown in Table 1. These are expected to be of increasing complexity for the reduced model since the temperature effect over the thermal properties is ever increasing with q_0.

Table 1. Description of the numerical experiments performed.

TEST #	q_0 $[\mathbf{W/m^2}]$
1	10^6
2	5×10^6
3	10^7

At last, all numerical experiments are 5 s long. The time stepping for solving the reduced model within the Kalman filter is $\Delta t = 0.02$ s, in a 24×24 numerical grid in the FVM discretization. The synthetic measurements were obtained from a grid- and timestep-independent solution of the complete model. Thus, the results presented herein are devoid of

inverse crime. The standard deviation considered in the simulations were $\sigma_y = 1.25$ K for the observation model and $\sigma_T = 1$ K and $\sigma_q = 10^5$ W/m^2 for the evolution model.

4.1.3 Computational resources

Computer codes were written in Fortran90 language to solve both the forward and inverse problems. The former was verified against simulations performed using COMSOL Multiphysics software, while the latter was verified using the Inverse Toolkit (ITK) database for inverse problems (Pacheco, 2022). The Intel Fortran compiler was employed for such tasks and all linear algebra operations were carried out using the BLAS and LAPACK packages contained in the Intel Math Kernel Library (MKL). Finally, Eq. (26) is a Discrete Algebraic Ricatti Equation (DARE) (Simon, 2006), so that the SLICOT numerical library (Benner et al., 1999) was used to achieve its solution. All simulations were run in an i7-9700KF with 3.60GHz and 16 GM of RAM. It is paramount to state that all the numerical experiments had a duration of 5 s, while the computer code solved the state estimation problem in about 3 s, using the methodology and codes developed by Pacheco *et al.* (2016).

4.2 Numerical experiment #1 – 10^6 W/m^2

For the sake of brevity, the results are analyzed herein by focusing on the temporal behavior at the core of the heated region. Figure 3 and Figure 4 show the results without and with KT in the reduced model. In both figures, the exact, experimental (synthetic) and estimated temperatures are compared, while for the heat flux the exact and estimated values are shown. In both cases, the estimates are presented with their respective 99% confidence intervals (CI).

In this numerical experiment, it is observed that both the reference temperature and heat flux values are successfully tracked in both scenarios. This means that in this case, including the KT does not bring significant advantage, as the reference heat flux is quickly encapsulated by the estimated heat flux and its 99% confidence interval. The residuals for these experiments are omitted herein for the sake of brevity, but it can be inferred from the temperature results that they are uncorrelated, oscillating around zero. Further analyses show that these residuals have the same order of magnitude of σ_y.

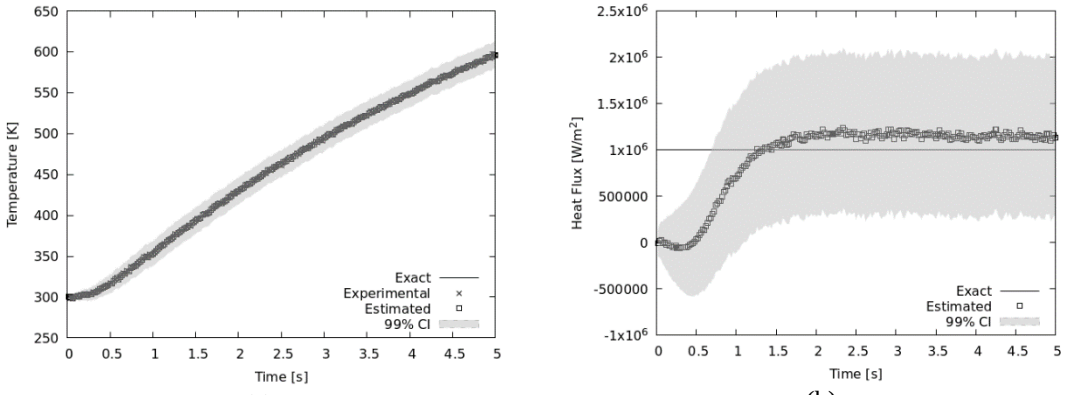

(a) (b)

Figure 3. Obtained results for numerical experiment #1 without Kirchhoff Transform: (a) temperatures; and (b) heat flux.

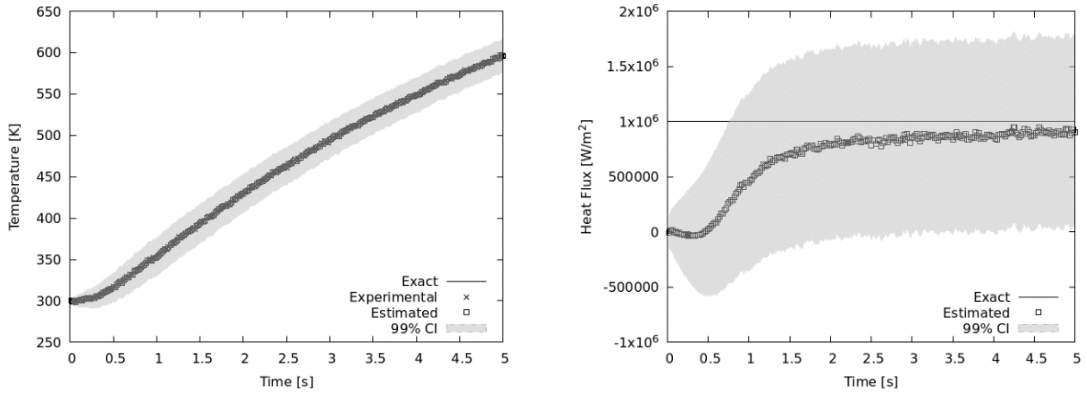

(a) (b)

Figure 4. Obtained results for numerical experiment #1 with Kirchhoff Transform: (a) temperatures; and (b) heat flux.

4.3 Numerical experiment #2 – 5×10^6 $\mathbf{W/m^2}$

The results for the second numerical experiment are shown in Figure 5 and Figure 6, without and with KT in the reduced model. When heat fluxes this strong are present, the limitations of the reduced model are unveiled, thus being insufficient to estimate the reference heat flux. Despite successfully reaching the reference values around 1.5 s, the estimates soon begin to decrease steadily. This can be understood physically through observation of the temperature values achieved: the increased temperature range results in significant changes in the thermal properties, causing the loss of accuracy in the estimates. This is confirmed by bearing attention to the temperature values in Figure 5, wherein the exact and experimental values are closely tracked by the estimated temperature and its 99% CI.

On the other hand, including the KT in the analysis now yields a noticeable improvement in performance. Figure 6 shows that the reference heat flux is enclosed by the estimate mean and CI and remains so throughout the numerical experiment. This evidences that the proposed modification in the reduced model resulted in an improved representation of the physics capable of accommodating the reflexes of the large temperature ranges in the thermal properties. Moreover, the exact and experimental temperatures remain closely tracked by the estimate mean and CI, again indicating that the residuals are expected to be oscillating around zero, with the same order of magnitude of σ_y. A closer analysis of these residuals supports this observation.

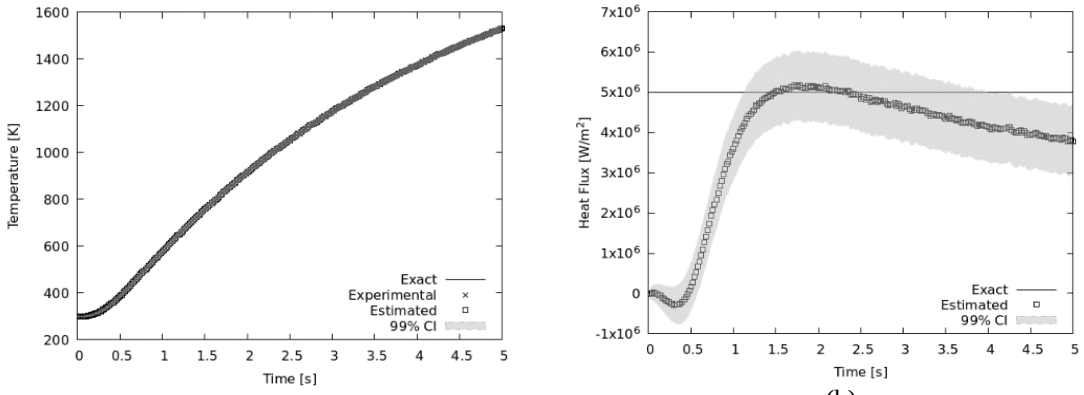

(a) (b)

Figure 5. Obtained results for numerical experiment #2 without Kirchhoff Transform: (a) temperatures; and (b) heat flux.

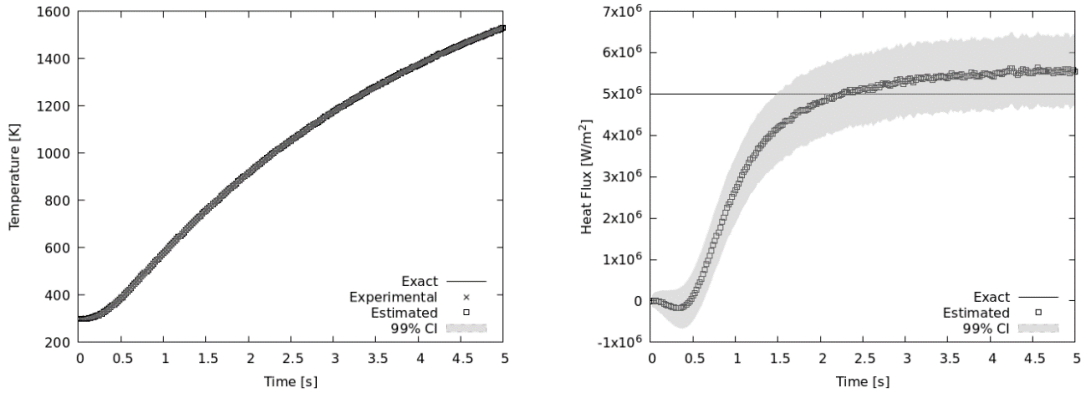

(a) (b)

Figure 6. Obtained results for numerical experiment #2 with Kirchhoff Transform: (a) temperatures; and (b) heat flux.

4.4 Numerical experiment #3 – 10^7 $\mathbf{W/m^2}$

In this last numerical experiment, the heat flux intensity is increased tenfold, to what is considered to be a very high heat flux. The results are shown in Figure 7 Figure 8, without and with KT, respectively. The lacking performance observed above in the absence of KT is now clearer, for the estimates mean and CI barely encapsulates the exact values around $t = 1.5$ s, decreasing steadily thereafter, despite the respective temperature values – both exact and experimental – being closely tracked by the estimates mean and CI. This supports an already existent expectation, that the even larger temperature range shown herein led to severe loss of adherence from the reduced model, which resulted in very poor estimates. Once again, the temperature values show that the exact and experimental values were closely tracked by the estimates mean and CI.

In Figure 8, it is shown that including KT in the reduced model significantly improves the performance, although it falls short of estimating the heat flux correctly. The estimates reproduce a constant heat flux 20% above the reference

value, which is kept throughout the remainder of the numerical experiment. This inconsistency may be explained by closely analyzing the inclusion of KT in the reduced model. It bears noticing that application of KT in the reduced model still requires the thermal diffusivity $\alpha(T)$ to be approximated by a constant value $\alpha^* = \alpha(T^*)$. And by its definition, together with observing Eqs. (5) and (6), it can be observed that the thermal diffusivity is somewhat linear with respect to temperature. That is, including KT in the reduced model indeed increase its robustness but only so far as α^* remains a good approximation for $\alpha(T)$. This allows for some variation in C and k, as long as their ratio is approximately constant.

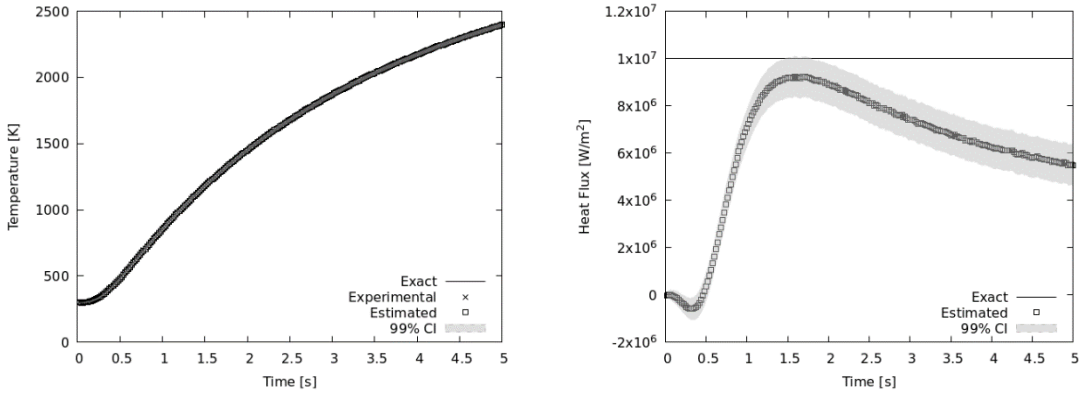

(a) (b)

Figure 7. Obtained results for numerical experiment #3 without Kirchhoff Transform: (a) temperatures; and (b) heat flux.

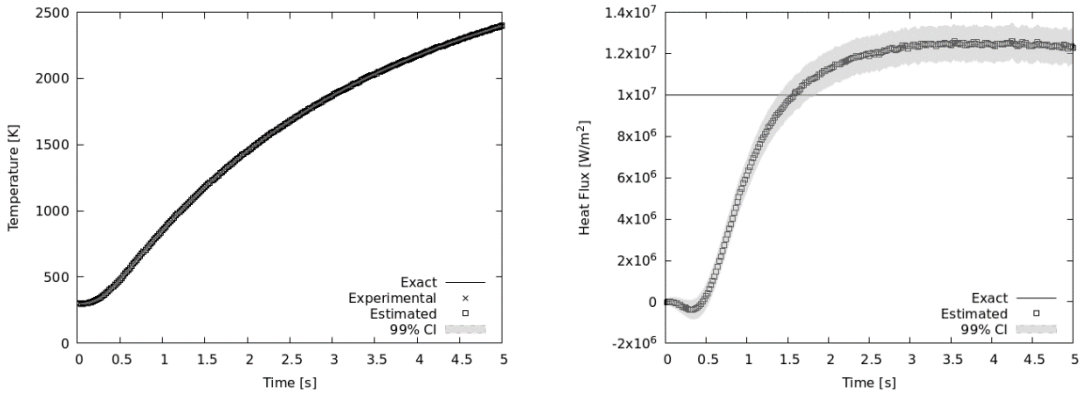

(a) (b)

Figure 8. Obtained results for numerical experiment #3 with Kirchhoff Transform: (a) temperatures; and (b) heat flux.

5. CONCLUSIONS

This paper presented a modification to the methodology developed by Orlande et al. (2013) wherein the reduced model was improved by including the Kirchhoff Transform to better account for variations in the thermal properties due to the large temperature range involved. This improved reduced model indeed increased the performance of the state estimation for high magnitude, focused heat fluxes, providing estimates with good agreement between reference and estimated quantities. Despite bringing important betterments for very high heat fluxes, the method still faces great challenges past a certain heat flux threshold – about 10^7 $\mathrm{W/m^2}$, meaning that improvements are still required if even stronger heat fluxes are to be estimated in this framework. Selecting different reference temperatures for calculating α^* might emerge as short-term solutions, but at the risk of hindering the state estimation at earlier times. Verily, the strides made so far, especially on reducing the computational effort, together with the findings presented herein evidence the proposed methodology as extremely promising for solving complex, nonlinear inverse heat conduction problems at real-time.

6. ACKNOWLEDGEMENTS

The authors would like to thank the Carlos Chagas Foundations for Fostering of Science in the State of Rio de Janeiro (FAPERJ) for the financial support of this work through the grants E-26/211.271/2019 and E-26/201.288/2021.

7. REFERENCES

Abdoli, A., Dulikravich, G.S., Vasquez, G., Rastkar, S., 2015. Thermo-Fluid-Stress-Deformation Analysis of Two-Layer Microchannels for Cooling Chips With Hot Spots. Journal of Electronic Packaging 137. https://doi.org/10.1115/1.4030005

Benner, P., Mehrmann, V., Sima, V., Van Huffel, S., Varga, A., 1999. SLICOT-A Subroutine Library in Systems and Control Theory, in: Datta, B. (Ed.), Applied and Computational Control, Signals, and Circuits SE - 10. Birkhäuser Boston, pp. 499–539. https://doi.org/10.1007/978-1-4612-0571-5_10

Chen, Z., 2003. Bayesian filtering: From Kalman filters to particle filters, and beyond. Statistics 182, 1–69. https://doi.org/10.1080/02331880309257

Cotta, R.M., Mikhailov, M.D., 1997. Heat Conduction: Lumped Analysis, Integral Transforms, Symbolic Computation. Wiley, Chichester; New York.

Hadamard, J., 1902. Sur les problèmes aux dérivées partielles et leur signification physique. Princeton University Bulletin 13, 49–52.

Huttunen, J., Kaipio, J., 2007. Approximation error analysis in nonlinear state estimation with an application to state-space identification. Inverse Problems 23, 2141.

Kakac, S., Yener, Y., Naveira-Cotta, C.P., 2018. Heat Conduction. Taylor & Francis Group.

Kalman, R.E., 1960. A new approach to linear filtering and prediction problems. Transactions of the ASME--Journal of Basic Engineering 82, 35–45. https://doi.org/10.1115/1.3662552

Orlande, H.R.B., Colaço, M.J., Dulikravich, G.S., Vianna, F.L.V., da Silva, W.B., Fonseca, H.M., Fudym, O., 2012. State Estimation Problems in Heat Transfer. International Journal for Uncertainty Quantification 2, 239–258. https://doi.org/10.1615/Int.J.UncertaintyQuantification.2012003582

Orlande, H.R.B., Dulikravich, G.S., Neumayer, M., Watzenig, D., Colaço, M.J., 2013. Accelerated Bayesian Inference for the Estimation of Spatially Varying Heat Flux in a Heat Conduction Problem. Numerical Heat Transfer, Part A: Applications 65, 1–25.

Ozisik, M.N., Orlande, H.R.B., 2021. Inverse Heat Transfer: Fundamentals and Applications, 2nd ed. CRC Press, Inc., Boca Raton, USA.

Pacheco, C.C., 2022. An online database of benchmark problems for verification of inverse problems computer codes. Presented at the International Conference on Inverse Problems in Engineering (ICIPE), Francavilla Al Mare, Italy.

Pacheco, C.C., Orlande, H.R.B., Colaço, M.J., Dulikravich, G.S., 2016. Real-time identification of a high-magnitude boundary heat flux on a plate. Inverse Problems in Science and Engineering 24, 1–1679. https://doi.org/10.1080/17415977.2016.1195829

Pacheco, C.C., Orlande, H.R.B., Colaço, M.J., Dulikravich, G.S., 2015. Estimation of a location-and-time dependent high magnitude heat flux in a heat conduction problem using the Kalman filter and the approximation error model. Numerical Heat Transfer, Part A 68, 1198–1219.

Reddy, S.R., Dulikravich, G.S., 2017. Inverse Design of Cooling Arrays of Micro Pin-Fins Subject to Specified Coolant Inlet Temperature and Hot Spot Temperature. Heat Transfer Engineering 38, 1147–1156. https://doi.org/10.1080/01457632.2016.1239924

Simon, D., 2006. Optimal State Estimation: Kalman, H Infinity, and Nonlinear Approaches. John Wiley & Sons, Inc.

Versteeg, H.K., Malalasekera, W., 2007. An Introduction to Computational Fluid Dynamics: The Finite Volume Method, 2nd ed. Longman Group Ltd.

8. RESPONSIBILITY NOTICE

The authors are the only ones responsible for the printed material included in this paper.